

# Строительные материалы и изделия

Construction Materials and Products

ISSN 2618-7183

journal homepage: https://bstu-journals.ru



DOI: 10.58224/2618-7183-2024-7-5-10

# Assessment of the influence of building parameters on the urban heat island in the districts of Moscow

Le M.T. <sup>1</sup>, Bakaeva N.V. \*<sup>1</sup>

<sup>1</sup> National Research Moscow State University of Civil Engineering, Russia

Abstract. Large cities, as financial centres, attract a dense adult population, leading to a high demand for housing. This growth requires urban expansion and increased building density, which disrupts the ecosystem and gives rise to a concentrated urban heat island (UHI). In a study conducted in Moscow, a numerical climate simulation model was used to explore the relationship between urban indices, specifically the building height-to-width ratio (H/W), sky view factor (SVF), and UHI intensity. The results indicated significant impacts of both H/W and SVF on UHI. More accurate predictions were achieved by adjusting coefficients in the Oke model using non-linear regression of simulated H/W and heat island intensity. These findings highlight the crucial role of urban morphology in UHI formation and development, providing a scientific basis for mitigating UHI impacts through urban planning strategies. While it is challenging to generalise a formula for calculating UHI intensity due to the diversity of urban forms, our research method offers a valuable approach for similar studies in other cities.

**Keywords:** local climate zone (LCZ), urban heat island, urban parameters, sky view factor (SVF), ENVI-met, environmental safety management

**Please cite this article as:** Le M.T., Bakaeva N.V. Assessment of the influence of building parameters on the urban heat island in the districts of Moscow. Construction Materials and Products. 2024. 7 (5). 10. DOI: 10.58224/2618-7183-2024-7-5-10

# 1. INTRODUCTION

Urban microclimates are shaped by the interplay of urban morphology, including building density, vegetation cover, surface materials, and local variations in meteorological conditions. As cities expand to accommodate growing populations, they become increasingly susceptible to heat waves and other climate extremes. Urban heat islands are one of the most extreme manifestations of urbanization. The formation of urban heat islands is attributed to replacing natural land cover with impermeable surfaces with low albedo, high heat capacity, and high thermal conductivity. Additionally, urban areas exhibit reduced latent heat flux and increased heat absorption [1]. In addition, the morphology of urban

\*Corresponding author E-mail: natbak@mail.ru

surfaces, characterized by buildings and narrow streets, significantly reduces overall wind ventilation due to increased surface roughness and more excellent heat retention caused by reflection within urban canyons [2, 3]. The heat generated by human activities contributes to the increase in heat accumulation [4]. The urban heat island effect has many direct or indirect impacts on the thermal comfort of residents [5, 6, 7]. In numerous urban centres worldwide, the urban heat island (UHI) affects residents by increasing heat stress and heat-related health issues, particularly during scorching summer months. Heat waves exacerbate these risks, leading to higher mortality rates from heat-related illnesses [8], [9] Previous studies have demonstrated that the UHI effect interacts with heat waves, prolonging and intensifying hot conditions [10, 11].

Numerous studies have examined the relationship between surface temperature and neighbourhood or block-scale urban characteristics, such as impervious surface area, building density, and street canyon geometry [3, 12, 13]. Researchers have also quantified the intensity of UHI at the neighbourhood scale based on the relationship between temperature and urban form [14, 15]. Past research has provided insights into the physical mechanisms underlying urban heat island formation and has suggested potential mitigation strategies.

Moreover, various urban form parameters (street networks, building plot characteristics, land use, natural features, and urban growth) can influence the spatial pattern of urban [16]. One study highlighted a strong correlation between the urban sky view factor and UHI [17], while others have indicated the impact of building density and vegetation in either exacerbating or mitigating the UHI effect [18, 19].

However, mitigation strategies such as green roofs and urban green spaces only have localised microclimate impacts [20]. As a result, rapid urban expansion poses significant challenges to mitigating urban heat. Nevertheless, it presents a crucial opportunity to apply urban climate knowledge in newly developing areas. Quantitative assessments are essential to support urban planning that considers the UHI effect.

When considering urban morphology and microclimatic parameters, research on the urban heat island (UHI) effect reveals a complex problem involving numerous urban variables. Previous studies have primarily compared surface temperatures between urban centres and suburban areas [21]. To address the limitations of these studies, Oke and Stewart [1] developed a local climate zone (LCZ) classification system incorporating detailed urban form and surface cover variations. This system provides a more quantitative approach to UHI research. However, the complexity of urban heat islands necessitates using numerical climate models and computational power to analyze the interactions between various urban parameters.

According to [22], urban heat islands, poor air quality, and reduced livability are direct consequences of limited open space, inadequate green infrastructure, and high-density development. Researchers have been actively engaged in studying the urban heat island phenomenon and exploring effective mitigation and adaptation strategies [23, 24]. In traditional research methods, the investigation of urban microclimates has been conducted primarily through measurement and observation [25]. Recent decades have witnessed remarkable progress in computational power, facilitating the application of computational fluid dynamics and heat balance modelling in simulations [26]. The development of numerical urban microclimate models relies on thoroughly understanding the intricate interactions between urban morphology, local climate, and energy exchanges, especially solar radiation and heat transfer from urban surfaces [27]. Some climate simulation models are limited in that they only consider solar radiation and ignore the significant impact of airflow through urban canyons [28, 29]. Large eddy simulation (LES) is used in some models to resolve fluid flow around individual buildings in urban canyons. However, due to its high computational cost, some urban models opt for the Reynolds-Averaged Navier -Stokes (RANS) equations, which offer a reasonable level of accuracy for radiation modelling while being more computationally efficient [30]. Modelling methods such as RANS, FLUENT, OpenFOAM, and StarCCM+ are considered complex computational tools requiring advanced user training [31]. While tools like RANS, FLUENT, and OpenFOAM require advanced training, tools like ENVI-met and SOLWEIG are more accessible to a broader range of users [32].

Studies on urban microclimate modelling consistently highlight ENVI-met as the leading model, citing its optimal balance of complexity, user-friendliness, and computational efficiency [33, 34], [35].

Moreover, ENVI-met is a dynamic atmospheric model that captures the evolving relationships between vegetation, atmosphere, and soil moisture. The model's high spatial resolution of approximately 2 meters per grid cell allows for detailed simulations at the neighbourhood scale.

ENVI-met is a Ruhr University Bochum model developed by Michael Bruse [36]. ENVI-met is a RANS-based CFD model that simulates atmospheric flow and heat transfer in urban areas. The model, now in its 5.6.1 version, offers a user-friendly interface and the capability to model complex urban geometries and vegetation, including vehicular emissions and water body evaporation. A typical validation approach for ENVI-met involves comparing simulated air temperatures with observations from a limited number of sites within the study area [37, 38].

The local climate is influenced by a combination of thermal processes, including macroclimate, topography, season, and time of day. While these factors are primarily fixed, urban planning and design can impact the local climate by integrating green infrastructure and spaces and making thoughtful material choices. The physical form and structure of cities, known as urban morphology, also significantly affect the urban thermal environment through factors such as building orientation, street layout, and open space distribution.

Strategies to mitigate the Urban Heat Island effect, such as urban greening, including street trees, parks, and water bodies, are prioritised as cooling solutions [39, 40, 41, 42]. The use of green infrastructure for urban cooling requires careful consideration. While it provides benefits such as shade and biodiversity, factors such as obstructed airflow and the impact of humidity on human thermal comfort need to be considered [43]. Less explored and understudied aspects of urban morphology in the context of urban cooling [44].

This study is based on the hypothesis that urban morphology, along with microclimate, plays a significant role in the formation of urban heat islands. The goal of the research is to use the ENVI-met model to assess urban heat islands by considering urban morphological factors.

#### 2. METHODS AND MATERIALS

2.1 An assessment of the current ecological, planning, and development conditions in Moscow

In the 1960s and 1970s, urban planning policies in Moscow aimed to limit the concentration of production and population in the capital and its immediate suburbs. Instead, they promoted the development of peripheral territories. To achieve this, forest park protection belts were established to prevent the consolidation of suburban development clusters and to create a unified system of green spaces within the city and surrounding areas. A construction ban was imposed on all adjacent territories within a radius of 50-60 kilometres from the Moscow Ring Road.

In 1971, a new General Development Plan for Moscow was adopted, focusing on creating a green belt. This resulted in a 6,000-hectare increase in the city's green space. Moscow's territory expanded to 87,500 hectares (compared to 35,000 hectares under the 1935 plan) and was surrounded by a 180,000-hectare protective forest park belt, 10-15 kilometres wide, emphasising northward development.

The green belt was an integral part of the urban planning strategy for Moscow and its agglomeration. The 1971 General Development Plan for Moscow focused on limiting and regulating urban growth. By 1970, the green belt encompassed eleven cities in the Moscow Region, with a population of over 1 million, and included seven administrative districts.

The 1971 General Development Plan for Moscow highlighted the importance of enhancing the natural environment by increasing green spaces by 1.5 times, canalising rivers, and creating new water bodies. The plan aimed to relocate over 300 enterprises and organisations outside the city limits, including industrial facilities, research and design organisations, and agricultural enterprises. However, the relocation of industrial facilities from Moscow was not successful, with only 20% of the total number being relocated. Similarly, the program to remove hazardous substances from Moscow also failed to achieve the expected results in reducing the number of workers and employees.

Furthermore, the General Plan called for implementing principles to ensure compatibility between the biosphere and the urban environment. The plan proposed creating a natural framework for the city, a vital system of green spaces following the city's hydrological network. This framework was formed based on the principles of continuity, stability, and connectivity of natural territories within the urban context (Fig. 1).

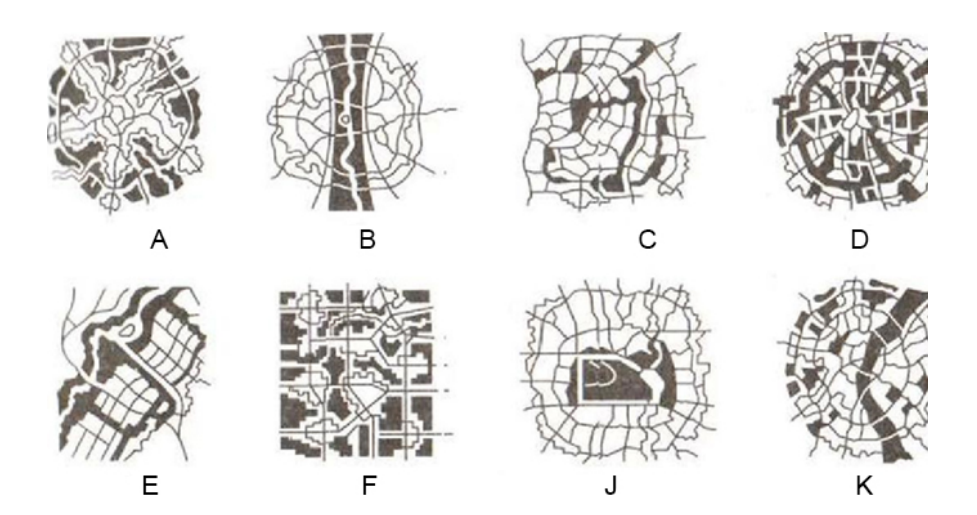


**Fig. 1.** Formation of the natural framework of the city: A) system of green wedges; B) diameter of blue water; C) system of green points; D) radial-ring system; E) system with a linear bandwidth; F) unique park environment with developed islands; J) compact, centralised system; K) combined system.

The natural framework of an urban ecosystem, as shown in Figure 1, encompasses specially protected areas, urban forests and parks, green spaces, and territories with specific use restrictions.

In 1985, it became evident that Moscow was facing several previously overlooked or considered insignificant issues. The increasing number of cars and industrial enterprises in the city were harming the environment. Concerns were raised for the first time about the significant damage caused to Moscow's natural surroundings. The Moscow region was still seen as an extension of the city, negatively impacting its infrastructure. It was clear that the pace of housing construction could not keep up with the growing demand—the new general plan aimed to address these issues gradually.

The mid-1980s saw the consolidation of Moscow and its surrounding areas into a single metropolitan region. This enabled more balanced road and public transport infrastructure development, especially in suburban areas. New growth centres, including Dmitrov, Noginsk, and Naro-Fominsk, emerged on the outskirts of Moscow and were linked to the city by railway lines.

The latest Moscow general plan introduced a radical shift in urban planning. It discarded the concept of horizontal transportation corridors in favour of a two-belt system, which eventually evolved into the Third Ring Road. The plan also addressed the city's ageing housing stock, proposing demolishing outdated five-story buildings and replacing them with large-panel housing. Additionally, it aimed to reduce industrial activity within the city limits.

The 1989 general plan for Moscow, though considered unrealistic given the political turmoil of the time, was never officially replaced. As a result, the city's development in the 1990s was primarily shaped by this outdated and unadopted document.

The latest general plan currently being implemented was adopted in 1999. This document outlines a development strategy for the capital city until 2020. Although it is still too early to assess the full results, some notable points can be observed. For instance, the plan projected Moscow's population to reach 10-12 million by 2020, but this figure has already been surpassed. Unlike its predecessors, the 1990s general plan was significantly more humane, strongly emphasising creating a comfortable urban living environment and incorporating aesthetic elements into the city and its surroundings. A novel aspect of this plan is the precise definition of activities prohibited in some city regions. While this promotes more significant involvement of stakeholders in urban development, it also leads to decisions being predominantly driven by financial interests, often at the expense of the long-term well-being of Moscow's residents.

Since 2005, the Moscow government has been working on a new general plan for the city. The plan incorporates green zones, although they are smaller, and some have been built without proper urban planning. Construction has also intruded upon parts of the green belt, diminishing Moscow's connection to its natural surroundings.

The new General Plan of Moscow, approved on May 5, 2010, and last amended on March 15, 2017, sets the course for the city's development until 2025. This document enables the intensification of land use in the central zone of Moscow, thus preserving the maximum amount of green spaces in the areas adjacent to the Moscow Ring Road. This compensates for reducing undeveloped land in the former suburban zone of the capital.

In 2012, the "New Moscow" project was initiated to tackle the issues of overpopulation and traffic congestion in Moscow. The city's area expanded by 1,548 square kilometres, resulting in a total area of 2,500 square kilometres. The newly added territories have different ecological conditions, population densities, land-use histories, and development strategies compared to the older parts of the city. For example, prior to 2012, over 80% of the New Moscow territory was covered by forests and farmland. This unique characteristic offers sustainable urban development and environmental preservation opportunities within the megaregion.

In 2015, the city authorities permitted developers to undertake any activities at their discretion in specially protected green areas, whereas previously, only activities directly related to conservation and research were allowed. Additionally, they gained the authority to modify the boundaries of specially protected green areas and establish their usage regimes without needing a Moscow government decision. Furthermore, the city authorities were granted the power to exclude certain lands within Moscow from the category of specially protected green areas.

#### 2.2 Research area

Moscow, the northernmost megacity in the world, is known for its vast urban sprawl. The Moscow Ring Road, a circular transportation artery with a radius of approximately 17 kilometres, defines the city's core. However, the city's spatial extent has significantly expanded beyond this boundary, especially in the northern and southern directions (Fig. 2).

Observational data from the TROICA project (2000-2010) verified the presence of an urban heat island effect in Moscow [45]. Moscow, a densely populated megacity, was home to approximately 13.01 million people in 2021, with an average population density of 5080 individuals per square kilometre. The city is on a flat plain, with an elevation between 110 and 255 meters above sea level.

The study focused on two districts of Moscow (Fig. 2), employing simulation modelling to evaluate the urban heat island:

- Zamoskvorechye is situated on the southern bank of the Moskva River, opposite the Kremlin and the city centre. This location makes the district an integral part of Moscow's general plan as a link between the central and southern districts of the city. It is one of Moscow's historic districts, possessing significant cultural and architectural value. Geographically, the district is located south of the Moskva River, bordered by the Moskva River to the north, Zhitnaya Street to the south, Sadovaya-Karetnaya Street to the west, and the Vodootvodny Canal to the east. Zamoskvorechye district covers an area of approximately 4699 km² and has a population of about 55,293 people (as of January 1, 2024). This district is notable for its numerous buildings in the classical architectural style, primarily from the 18th and 19th centuries. The district is also home to many ancient churches and monasteries. Zamoskvorechye's public transportation system is well-developed, including metro, buses, and trams. The Zamoskvorechye district is one of Moscow's most diverse districts, where the past and the present collide, creating a unique and attractive living environment. The district's planning and architecture reflect a respect for cultural heritage and a striving for a sustainable and modern future.

- Konkovo is a district located in the southwest of Moscow, within the South-West Administrative Okrug of Moscow, Russia. It is a popular residential area with developed infrastructure and convenient transportation links. Konkovsky District has an area of approximately 3.49 km² and borders Yasenevsky, Tepliy Stansky, and Belyaevsky Districts. The population of Konkovo is approximately 152,544 (as of January 1, 2024). The residents here are mainly Russians, with a small number of foreigners. The Konkovo district has a metro station, "Konkovo", of the Kaluzhsko-Rizhskaya metro line, which connects the district with the centre of Moscow and other city areas. In addition to the metro, the area also has a network of buses and trams serving the transportation needs of the residents. The Konkovo district of Moscow has a layout and architecture that reflects typical Moscow urban development of the Soviet era and more modern adaptations of recent years. Before this, the area consisted mainly of villages and agricultural land. The development of the Konkovo district is predominantly multi-apartment high-rise buildings built in the Khrushchevka and Brezhnevka styles.

These buildings are often simple in design, emphasising the functionality of reinforced concrete structures. These buildings are typically five to nine storeys high with compact but economical apartments. Since the late 1990s and 2000s, several more modern properties have been built, including luxury apartment buildings and shopping centres. Some new buildings have been constructed with more varied architecture, using modern materials and construction technologies to improve residents' quality of life. The layout and architecture of the Konkovo district reflect a combination of historical and modern elements, creating a diverse and attractive residential area of Moscow.

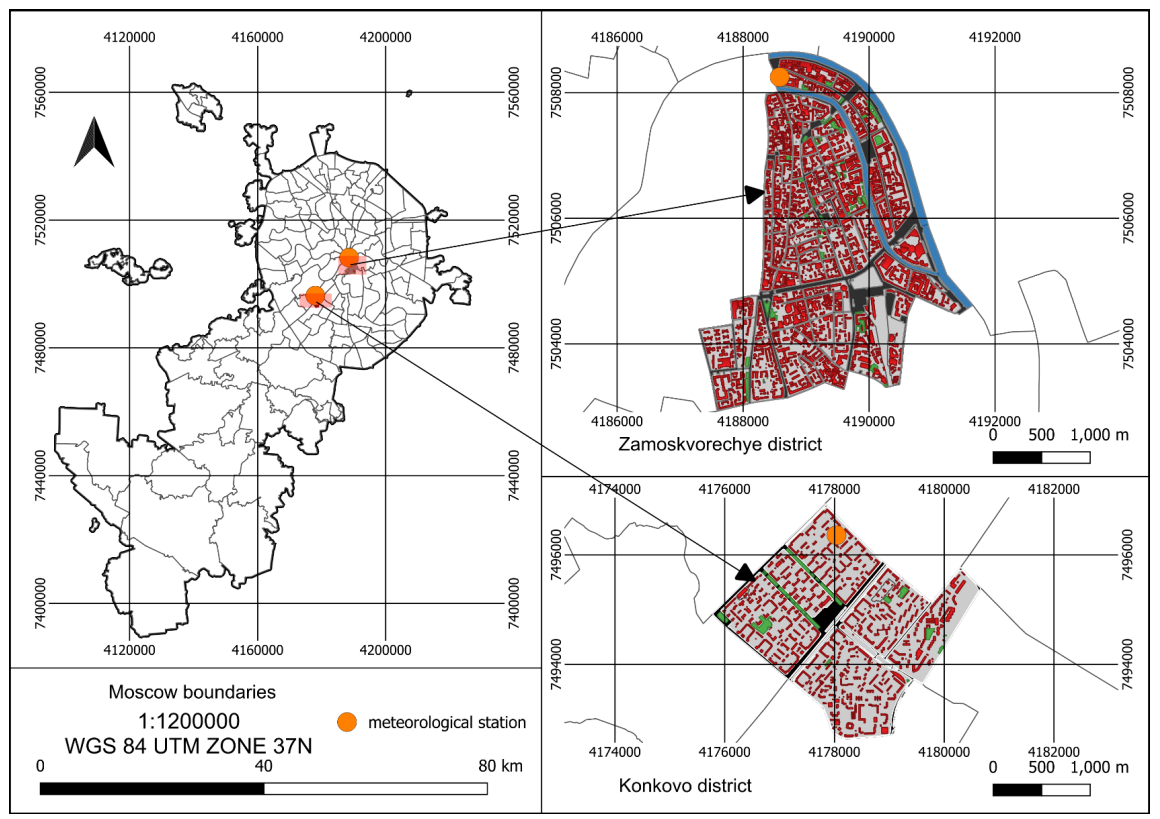


Fig. 2. The official territory of Moscow includes the city and its district areas.

2.3. Microclimate data for the study area in Moscow is being recorded by 'CityAir' weather stations

# 2.3.1. Description of the device used to measure microclimate values

The real-time microclimate monitor is an advanced environmental monitoring system designed to measure and monitor microclimate indicators in real time. The meter's sensors provide data on temperature, humidity, wind speed, and pressure in the device's location. The microclimate indicators used in the study were provided by the real-time microclimate monitor of the Russian Cityair meteorological monitoring stations (Fig. 3, Table 1). The device is an approved measuring instrument with state registration number 75984-19.



Fig. 3. The external appearance of the device for measuring microclimate values.

**Table 1.** Technical specifications of Cityair's real-time microclimate index monitor.

Name of the parameter	Meaning		
or characteristic			
Communication channels	GSM: GPRS (EGSM 900, DCS 1800)		
	Wi-Fi: b/g/n 2,4 ГГц		
	Ethernet: 10/100 BASE-T/TX		
Navigation systems	GPS, GLONASS		
Level of protection	IP56		
Overall dimensions	160 × 320 × 465 mm		
Weight	10 kg		
Autonomous work	24 hours		
Data storage buffer	upto 30 days		

2.3.2. Actual microclimate data collected by 'CityAir' weather stations within the Moscow study

Real-time microclimate data obtained from existing Cityair stations in Moscow on June 4, 2021, were used as input for the simulation model. The values are presented in Table 2.

**Table 2.** Microclimate data collected by CityAir stations in Moscow during 24 hours on June 4, 2021, were used as input for numerical modelling.

Weather station address	Balchug Street, 5	Stroiteley street, 11	
Simulation model dimensions, m	2720 × 3460 × 250	3000 × 2550 × 226	
Model dimensions (the number of grids in XYZ directions)	272 × 346 × 27	300 × 255 × 26	
Grid cell dimensions, m, dx, dy, dz	10 × 10 × 10	10 × 10 × 10	
Geographical position (latitude, longitude)	55.74, 37.62	55.68, 37.53	
Sub-grids	10	10	
Vertical grid generation method	Equidistant	Equidistant	
Time zone	GMT +3	GMT +3	
Simulation date	June 04, 2021	June 04, 2021	
Simulation starts time and duration	00:00, 24:00 hours	00:00, 24:00 hours	
Wind velocity at the altitude of 10 m	1.9 m/s	1.9 m/s	
Wind direction	45°	45°	
Minimal temperature (simulation date)	16.29° <sup>℃</sup> , 4:00 am	14.31°C, 4:00 am	
Maximal temperature (simulation date)	23.73°C, 4:00 pm	20.02°C, 6:00 pm	
Unit humidity of the upper part of a model (2,500 m, g/kg)	9 g/kg	9 g/kg	
Minimal humidity (simulation date)	25%, 03:00 pm 45%, 04:00 pm		
Maximal humidity (simulation date)	61%, 3:00 am	75%, 4:00 am	

The ENVI-met database output files provide a rich collection of 3D materials and vegetation, enabling the detailed simulation of urban environments. Each material is defined by a unique set of parameters, including thermal capacity, absorptivity, and reflectivity, as illustrated in Fig. 4 and Table 3, which are crucial for constructing the terrain model.

**Table 3.** Types of elements in a built environment.

Element type	Albedo
Concrete wall	0,3
Paved road	0,2
Sidewalks	0,3
Soil	0,1

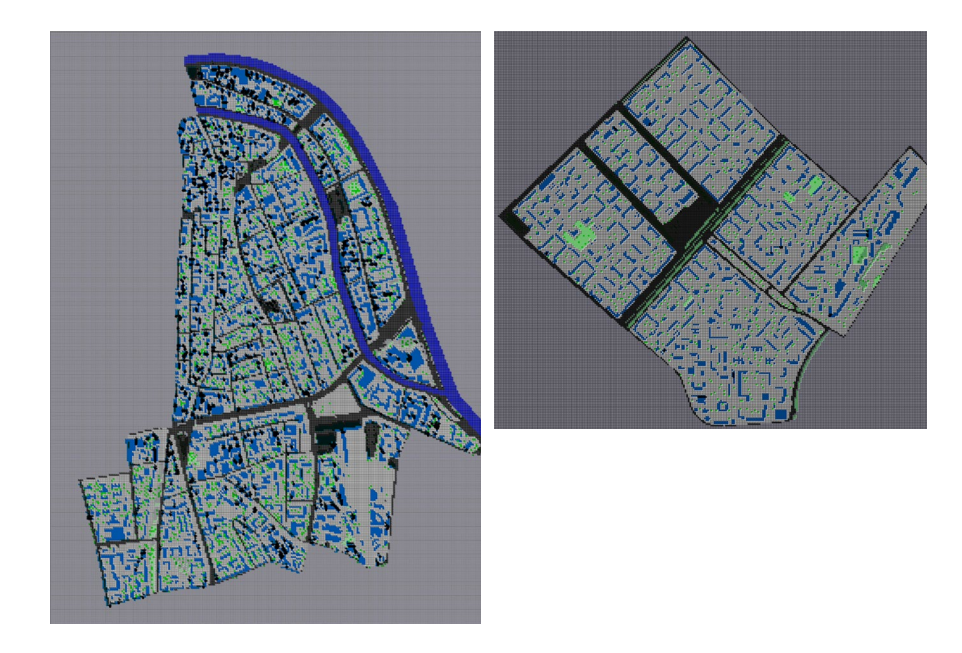


Fig. 4. Types of materials within an area under research (2D).

# 2.4. Numerical simulation model

ENVI-met, a user-friendly CFD modelling tool, is popular among researchers in urban fields. Founded on urban microclimate fluid dynamics, ENVI-met 5.6.1 (released in late 2023) employs RANS equations. Its intuitive interface enables researchers to set up a test domain and initiate simulations quickly.

ENVI-met is a three-dimensional microclimate model specifically developed for simulating the intricate interactions between surfaces, vegetation, and air in urban settings, as illustrated in Fig. 5.

The ENVI-met model is a collection of the following sub-models:

A 1D boundary layer model is used to initialise and define the boundary conditions for the 3D atmospheric model.

A 3D atmospheric model, in which temperature, humidity, wind flow, turbulence, shortwave and longwave radiation fluxes, as well as the dispersion and deposition of pollutants, are modelled.

A soil model in which surface temperature and the distribution of soil temperature and water balance is simulated.

A vegetation model, including simulations of transpiration rate, leaf temperature, and heat and water vapour exchange between vegetation and the atmosphere.

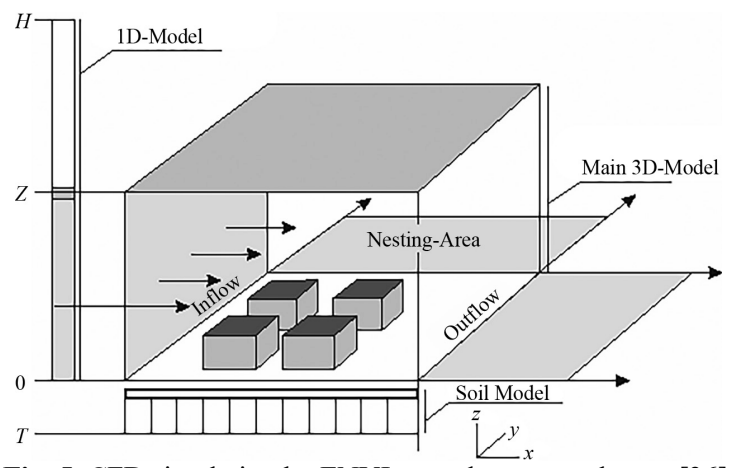


Fig. 5. CFD simulation by ENVI-met: the process layout [36].

ENVI-met, a model grounded in fluid dynamics and thermodynamics, offers precise simulations of diurnal cycles of vital climatic variables. ENVI-met can model temperature, humidity, soil moisture, wind, and radiation fluxes in detail by employing fine-scale horizontal resolutions of 0.5-5 meters and short time steps of 1-5 seconds [36]. The simulation necessitates 3D urban geometries as primary input data, encompassing buildings, roads, sidewalks, vegetation, and water bodies. Other essential inputs include albedo values, location parameters, microclimate data, and the simulation start time.

ENVI-met version 5.6.1 provides a forcing scheme for microclimatic input parameters such as wind, air temperature, radiation, and relative humidity, which involves defining hourly variations of these variables throughout the simulation period. This enables the model to achieve higher simulation accuracy and more realistic results [46]. Shortcomings have been identified in the overall calculation of radiative fluxes [34, 47] and the application of Yamada and Mellor's turbulence closure scheme. Specifically, these models tend to overestimate turbulence in regions of high acceleration [48], [49] neglect near-wall phenomena [48], and assume static cloud and wind conditions during simulations [50], which can compromise the reliability of the simulation results.

The study focuses exclusively on the fundamental equations of the physical model, omitting additional models like biometeorological and particle dispersion models.

Average airflow in ENVI-met model:

The fundamental equations for describing three-dimensional turbulent flow are the hydrostatic incompressible Navier-Stokes equations in the Boussinesq-approximated form (1.1, 1.2, 1.3) and the continuity equation (2):

$$\frac{\partial u}{\partial t} + u_i \frac{\partial u}{\partial x_i} = -\frac{\partial p'}{\partial x} + K_m \left(\frac{\partial^2 u}{\partial x_i^2}\right) + f(v - v_g) - S_u \tag{1.1}$$

$$\frac{\partial v}{\partial t} + u_i \frac{\partial v}{\partial x_i} = -\frac{\partial p'}{\partial y} + K_m \left(\frac{\partial^2 v}{\partial x_i^2}\right) - f(u - u_g) - S_v \tag{1.2}$$

$$\frac{\partial w}{\partial t} + u_i \frac{\partial w}{\partial x_i} = -\frac{\partial p'}{\partial z} + K_m \left(\frac{\partial^2 w}{\partial x_i^2}\right) + g \frac{\theta(z)}{\theta_{ref}(z)} - s_w \tag{1.3}$$

With 
$$u_i = (u, v, w), x_i = (x, y, z)$$
 for  $i = 1,2,3$ 

$$\frac{\partial u}{\partial x} + \frac{\partial v}{\partial y} + \frac{\partial w}{\partial z} = 0 \tag{2}$$

In the formula, f is the Coriolis parameter whose value is  $f = 10^4 sec^{-1}$ , p' Is the local pressure perturbation, and q is the potential temperature at level z. The reference temperature  $\theta_{ref}$  Represents the average scale conditions and is provided by a one-dimensional model running parallel to the main model. The local sink sources Su, Sv và Sw represents wind speed loss due to drag on vegetation elements. This effect can be parameterised by formula (3):

$$S_{u(i)} = \frac{\overline{\partial p'}}{\partial x_i} = c_{d,f} LAD(z). W. u_i$$
(3)

In which, W is the average wind speed at height Z, with a value  $W = (u^2 + v^2 + w^2)^{0.5}$  and  $LAD_{(z)}$ Is the leaf area density  $[m^2m^{-3}]$  Of trees at the same height as Z [51, 52]. Mechanical resistance coefficient at tree elements  $c_{d,f}$  Set value by 0,2.

Temperature and humidity in the ENVI-met model:

The temperature  $(\theta)$  and specific humidity (q) distributions within the atmosphere are calculated using the convective-diffusion equation combined with an internal source:

$$\frac{\partial \theta}{\partial t} + u_i \frac{\partial \theta}{\partial x_i} = K_h \left( \frac{\partial^2 \theta}{\partial x_i^2} \right) + Q_h \tag{4}$$

$$\frac{\partial q}{\partial t} + u_i \frac{\partial q}{\partial x_i} = K_q \left( \frac{\partial^2 q}{\partial x_i^2} \right) + Q_q \tag{5}$$

 $Q_h$  and  $Q_a$  Are used to relate heat and vapour exchange at the vegetation surface to the atmospheric model. The values of  $Q_h$  and  $Q_a$  Are determined by the vegetation model.

Vegetation in ENVI-met model:

Vegetation is considered a one-dimensional column of height Z<sub>p</sub>With normalized leaf area density (LAD) and root area density (RAD). This solution is very general and can be used for small plants such as grasses or crops and large trees.

The interaction between leaves and the surrounding air can be expressed in terms of direct heat flux  $(I_{f,h})$ , evaporation flux  $(I_{f,evap})$ , transpiration flux  $(I_{f,trans})$ :

$$I_{f,h} = 1. lr_a^{-1} (T_f - T_a) (6.1)$$

$$I_{f,evap} = r_a^{-1} \Delta q \delta_c f_w + r_a^{-1} (1 - \delta_c) \Delta q$$
(6.2)

$$I_{f,trans} = \delta_c (r_a + r_s)^{-1} (1 - f_w) \Delta q \tag{6.3}$$

The vegetation model is linked to the primary atmospheric model through the following equations:

$$Q_h(z) = LAD(z)J_{f,h}$$
(7)

$$Q_q(z) = LAD(z)(J_{f,evapo} + J_{f,trans})$$
(8)

Turbulence and exchange processes in the ENVI-met model:

The ENVI-met model builds the turbulence and exchange process on the theoretical foundation of Mellor and Yamada [53]. In addition, the accuracy is 1.5 times higher due to the addition of two equations for local turbulence (E) and its dissipation rate (e) for the model:

$$\frac{\partial E}{\partial t} + u_i \frac{\partial E}{\partial x_i} = K_E \left( \frac{\partial^2 E}{\partial x_i^2} \right) + Pr - Th + Q_E - \varepsilon \tag{9}$$

$$\frac{\partial \varepsilon}{\partial t} + u_i \frac{\partial \varepsilon}{\partial x_i} = K_{\varepsilon} \left( \frac{\partial^2 \varepsilon}{\partial x_i^2} \right) + c_1 \frac{\varepsilon}{E} Pr - c_3 \frac{\varepsilon}{E} Th - c_2 \frac{\varepsilon^2}{E} + Q_{\varepsilon}$$
 (10)

# 2.5. Local climate zone (LCZ)

Local climate zones were proposed in a studyđiuiem by [1] to classify urban forms based on climate. Local climate zones are defined as areas with homogeneous surfaces, structures, materials and

human activities extending from hundreds of meters to several kilometres horizontally [1]. Each LCZ is named and identified according to its parameters and characteristics. The basic parameters for identifying LCZs are based on urban height and surface cover. The physical characteristics of all zones can be measured based on digital urban models. Urban morphology analysis will use parameters such as building height (BH), building surface fraction (BSF, i.e. building coverage ratio), sky view factor (SVF) and aspect ratio (H/W); land cover parameters of pervious surface fraction (PSF) and impervious surface fraction (ISF); and street geometry parameter of street width (SW).

The average height of buildings is calculated by the formula [54, 55]:

$$BH = \frac{\sum_{i=1}^{n} Bfi * Bfh}{n} \tag{11}$$

BH: building height (m); Bf: is the number of stories in the i-th building; Bfh: story elevation (3 m); n: The total number of buildings in a parcel

Construction area BSF-Building surface fraction calculated by the formula [54, 55]:

$$BSF = \frac{\sum_{i}^{n} Bfa}{Pa} \tag{12}$$

BSF: building surface fraction; Bfa: building footprint area; n: the total number of buildings in a parcel; Pa: total parcel area

The H/W-Aspect ratio is one of the most difficult parameters to calculate because the building height and street width vary within the same street [54, 55]. Therefore, the H/W-Aspect ratio is calculated for each plot. The H/W ratio is usually divided into H/W< 0.75 and H/W> 0.75. The average H/W ratio is calculated by dividing the average building height by the average street width. The H/W ratio is calculated according to the formula [54, 55]:

$$H/W = \frac{BH}{SW} \tag{13}$$

H: height (m); W: width (m); BH: building height (m); SW: street width (m)

\* The average street width is calculated using a quadratic equation using the area and perimeter values of the "road" polygon. Solving the equation below will yield two solutions, the smaller positive value being the average street width.

$$2 * sw_{average}^2 - P_{road} * sw_{average} + 2 * S_{road} = 0$$
(13.1)

 $sw_{average}$ : average street width (m),  $P_{road}$ : perimeter of the street (m);  $S_{road}$ : area of the street (m2)

The SVF is the surface area of the resultant geometry divided by the hemisphere's surface area. Through intensive and diverse studies that have investigated SVF and its relationship with urban heat island (UHI), thermal comfort, energy budget, air temperature and daylighting. The SVF coefficient is calculated by the formula [54, 56]:

$$SVF = \frac{\sum_{i=1}^{n} SVFi}{n} \tag{14}$$

$$SVFi = \frac{SSky}{(SSky + \sum Sb)}$$
(14.1)

SVFi is the SVF value of a certain point in a non-building area (point area 1 m \* 1 m) in the LCZ sample site. n is the number of SVF points (1 m \* 1 m) in the non-building area of the site. S\_Sky and  $\Sigma$ Sb represent the area of the sky and the area occupied by buildings at a certain point, respectively. SSky+ $\Sigma$ Sb represents the entire hemispheric environment at a certain point.

Local climate types are classified in Table 4 based on the type of construction combined with the surface cover type.

**Table 4.** Classification of local climate zones [1].

Built types	Definition	Built types	Definition
LCZ 1. Compact high-rise	The area is densely populated with many highrise buildings, few trees, and various construction materials such as steel, concrete, stone, glass, and paved sidewalks.	LCZ 6. Open low-rise	The area has a spacious layout with a high concentration of buildings, including low-rise structures with 1-3 floors. construction materials include concrete, brick, and stone. The sidewalk has many layers of permeable soil.
LCZ 2. Compact midrise	The area includes medium-height buildings (3-9 floors), and construction materials include concrete, brick, and stone. Sidewalks are paved.	LCZ 7. Lightweight low-rise	The area has a compact structure, dense construction, one-story buildings, and light construction materials. Sidewalks are mainly hard soil.
LCZ 3. Compact low-rise	The area includes low-rise buildings (1-3 floors), and construction materials include concrete, brick, and stone. Sidewalks are paved.	LCZ 8. Large low-rise	The area has an open structure consisting of low-rise buildings occupying a large area (1-3 floors), no trees, materials including concrete, bricks, and stones. Sidewalks are mostly paved.
LCZ 4. Open high-rise	The area has an open structure of high-rise buildings; construction materials are concrete, stone, and glass. The sidewalk has many layers of permeable soil.	LCZ 9. Sparsely built	The area is sparsely populated with small to medium-sized buildings in a natural setting. The pavements have a variety of permeable soil layers.

#### Continuation of Table 4

LCZ 5. Open midrise	The area has an	LCZ 10. Heavy	The area consists of
_	open structure	industry	low-rise and mid-rise
	consisting of		industrial buildings,
N N N	medium-height	E L	no trees, and concrete
the steel steel	buildings (3-9	1 5	and steel construction
	floors);		materials. The land
	construction		cover is mainly
	materials include		asphalt or hard-
	concrete, brick,		packed.
	and stone. The		
	sidewalk has		
	many layers of		
	permeable soil.		

# 2.6. Urban heat island intensity on road surface

In Oke. T.R.'s studies on boundary layer climatology, a theory, have been developed from empirical evidence through physical scale modelling and observational data collected from the selected study area to analyse urban heat island formation. Based on mathematical logic, the researcher has developed an empirical numerical model. Equation 15 (with R2=0.89) for calculating the urban heat island intensity has become one of the most reputable references in urban climatology, as it demonstrates the relationship between the urban heat island and urban morphology through the equation:

$$\Delta t_{u-r} = 7.54 + 3.97 * \ln\left(\frac{H}{W}\right) \tag{15}$$

 $\Delta t_{u-r}$ : is the maximum urban heat island intensity;

H: is the height of the buildings in the urban canyon;

W: is the width of the street in the urban canyon.

# 3. RESULTS AND DISCUSSION

# 3.1. Geometric features of the urban study area

The urban form has a complex impact on the microclimate within metropolitan areas. High building density and limited sky view factors between structures slow surface cooling rates during clear, calm nights, leading to the urban heat island (UHI) phenomenon [3]. To quantify the urban geometric characteristics of the chosen study area, a suite of urban parameters was selected for computation and analysis.

Based on a Geographic Information System (GIS) and field surveys, a 3D simulation map was created, including detailed and accurate layers of roads, sidewalks, buildings, water bodies, trees, and grass. Building heights were classified into three levels based on the number of floors: low-rise buildings (1-3 floors), mid-rise buildings (3-9 floors), and high-rise buildings (10+ floors) (Figures 6 and 7). The area of each surface cover and the built-up area are presented in Table 5.

**Table 5.** Surface area of various types.

Area, km2	Built-up	Sidewalk	Roads	Green zone	Waterbody	Total
	area					
Zamoskvorechye	1.18	2.51	0.68	0.059	0.27	4.699
district						
Konkovo district	0.46	2.50	0.39	0.14	-	3.49

Table 5 data supports the assertion that urban areas generally exhibit high surface reflectivity and limited vegetation cover, primarily in open spaces and road networks.

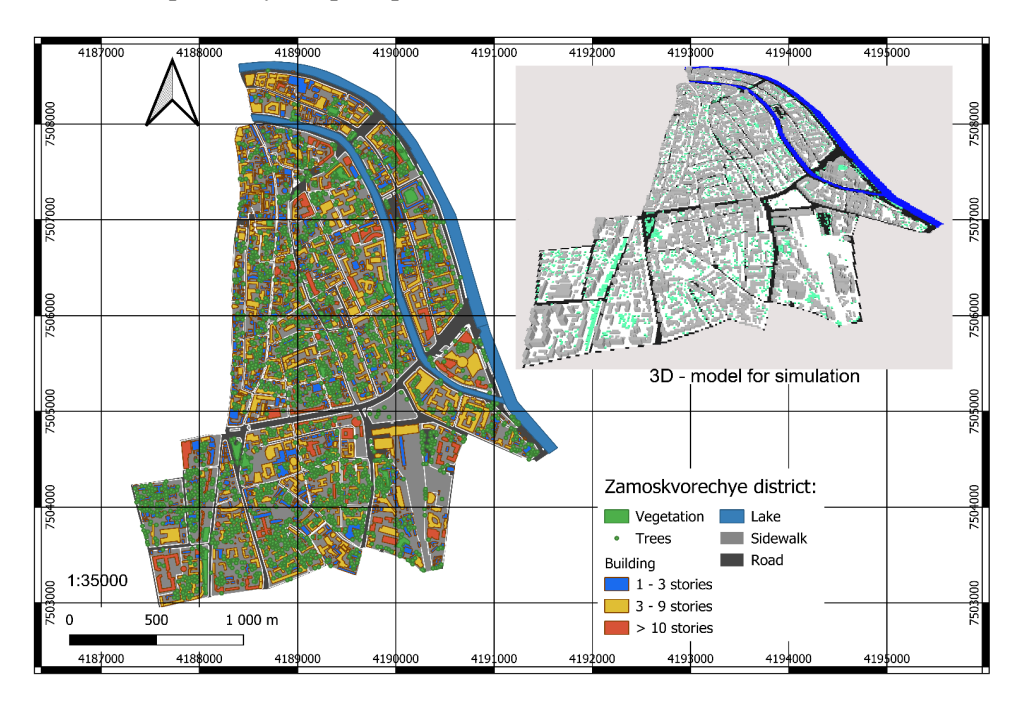


Fig. 6. A map classifying building heights and surface cover in the Zamokvorechye district.

Fig. 6 shows that mid-rise buildings (3-9 stories) dominate the district of Zamoskvorechye. Based on the characteristics described in Table 4 (local climate zone classification), Zamoskvorechye belongs to Local Climate Zone 2 (LCZ-2), which is characterised by medium-rise buildings (3-9 stories), construction materials such as concrete, brick, and stone, and paved sidewalks.

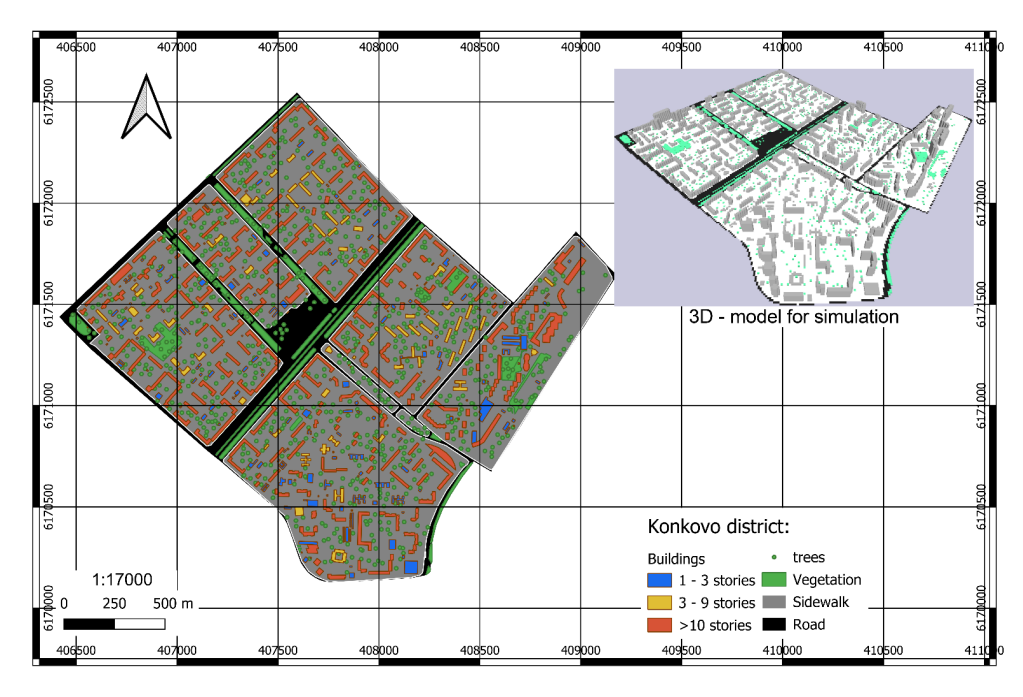


Fig. 7. A map classifying building heights and surface cover in the Konkovo district.

In Fig. 7, it can be seen that high-rise buildings (10+ stories) are predominant in the Konkovo district. According to the characteristics outlined in Table 4 (local climate zone classification), Konkovo falls into Local Climate Zone 4 (LCZ-4), which is characterized by a high-rise, open structure with concrete, stone, and glass buildings. The sidewalks are fitted with permeable paving.

Urban morphological parameters of the study area are tabulated in Table 6. The sky view factor (SVF) represents the proportion of the sky visible from a given point. A high SVF allows more sunlight to reach the ground, increasing temperature and irradiance. Conversely, a low SVF limits the amount of the sun and reduces temperature. Additionally, a high SVF allows for better air circulation, contributing to cooling and improved air quality.

Location	Skyview factor (SVF)	Areal aspect ratio (H/W)	Building surface fraction (BSF)
Zamoskvorechye district	0.08 - 0.82	0.69	0.32
Konkovo district	0.08 0.81	0.66	0.16

**Table 6.** Statistics of urban morphology parameters of the research area.

As indicated in Table 6, the sky view factor (SVF) in both Zamoskvorechye and Konkovo districts varies between 0.08 and 0.82, revealing the existence of both open spaces and areas with high-rise buildings that obstruct sky views. Furthermore, despite having a lower H/W ratio, Zamoskvorechye exhibits a Building Surface Fraction (BSF) nearly twice that of Konkovo. This implies a higher building density in Zamoskvorechye, potentially leading to challenges in infrastructure and the ecological environment. The spatial patterns of the sky view factor in both districts are visualised in Fig. 8.

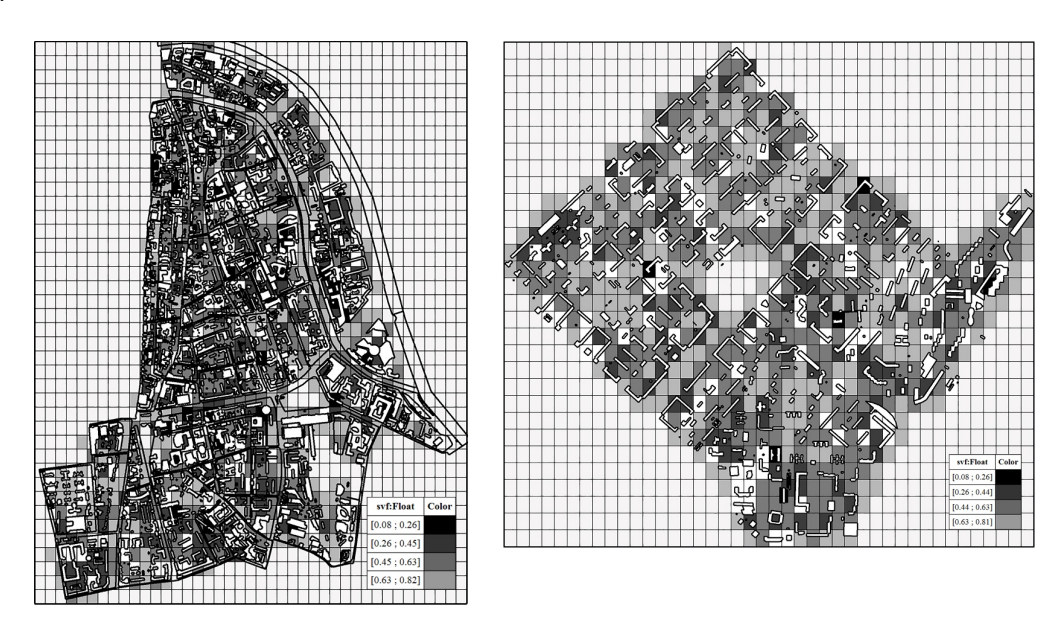
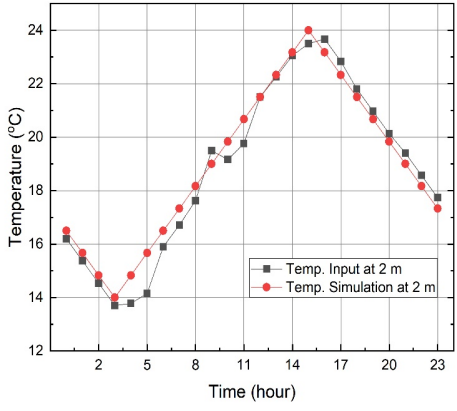


Fig. 8. A map showing the calculated sky view factor (SVF) for the Zamoskvorechye and Konkovo districts.

#### 3.2. ENVI-met simulation results

Due to the nonlinearity and complexity of modelling urban climate and thermal phenomena, dynamic numerical models are necessary for comparative analysis of the relative potential of different proposed measures and baseline scenarios. The R-squared value of 0.97, obtained by comparing the average temperature values from actual ground measurements with those obtained from modelling,

confirms the reliability of the calculations in ENVI-met for the selected area (Figs. 9, 10, 11, 12). ENVI-met has proven to be software capable of reproducing the complexity of the urban climate system. It simultaneously calculates and interacts with radiative, thermal, and hydraulic balances and aerodynamics in urban spaces at various scales. These calculations can be used to model the climate of Zamoskvorechye and Konkovo districts.



**Fig. 9.** The air temperature was measured at the station and simulated air temperature at 2m in the Zamoskvorechye district.

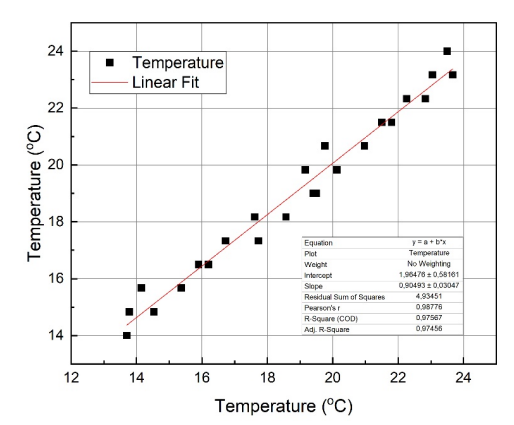


**Fig. 10.** Linear regression determining the accuracy of measured and simulated values of temperature of Zamoskvorechye district.

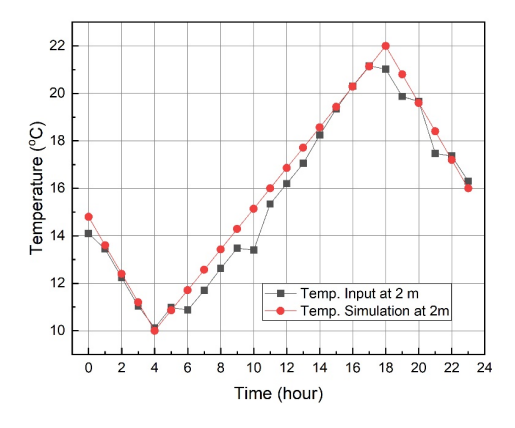


**Fig. 11.** The air temperature was measured at the station and simulated air temperature at 2m in the Konkovo district.

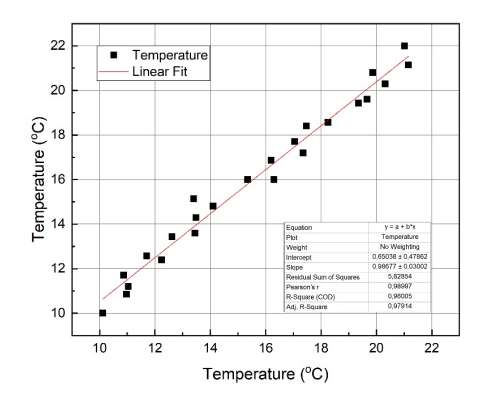
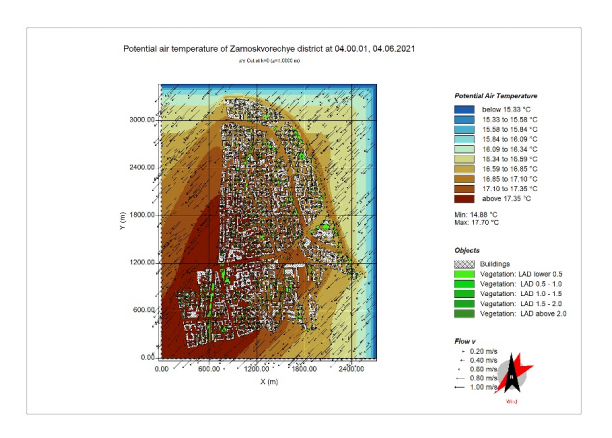


**Fig. 12.** Linear regression determining the accuracy of measured and simulated values of temperature of Konkovo district.

The ENVI-met program provides 24-hour microclimate simulation results for Zamoskvorechye and Konkovo districts on June 4, 2021. The simulated climate results have identified the hottest and most remarkable periods in both areas. For Zamoskvorechye, the most extraordinary period was at 4:00 AM (Fig. 13), with an average district temperature of 16.29 °C, and the hottest period was at 4:00 PM (Fig. 14), with an average district temperature of 23.73 °C, resulting in a temperature difference of 7.44 °C. For Konkovo, the most remarkable period was at 4:00 AM (Fig. 15), with an average district temperature of 14.31 °C, and the hottest period was at 6:00 PM (Fig. 16), with an average district temperature of 20.02 °C, resulting in a temperature difference of 5.71 °C. Both study areas have a predominant wind direction from the southwest. Due to the southwest wind direction, buildings on the southwestern side of both districts are significantly affected by the urban heat island effect. In addition to the hot southwest wind, urban morphology contributes to increased surface temperatures due to the suboptimal arrangement of green spaces and buffers. Zamoskvorechye has only 0.059 km² of green

space, while Konkovo has 0.14 km<sup>2</sup>. One of the main reasons for the much lower amount of green space and green buffers in Zamoskvorechye compared to Konkovo is that Zamoskvorechye is situated in the southern part of central Moscow and is one of the oldest districts in the city. As a result, the population has been concentrated and developed for a long time. Rapid urbanisation has gradually reduced green space and buffer areas to accommodate the high population density.



Potential air temperature of Zamonokovacchye district at 18,00 01, 04,00 2021

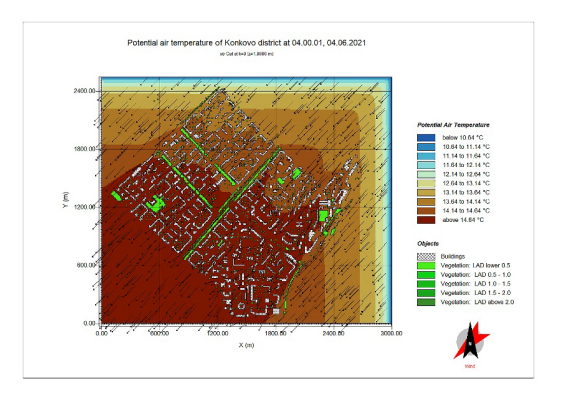
\*\*\*Observation Servation Confidence\*\*

\*\*Description of Confidence\*\*

\*\*Description Confide

**Fig. 13.** Potential air temperature of Zamoskvorechye district at 04.00 am, June 04, 2021 yr.

**Fig. 14.** Potential air temperature of Zamoskvorechye district at 04.00 pm, June 04, 2021 yr.



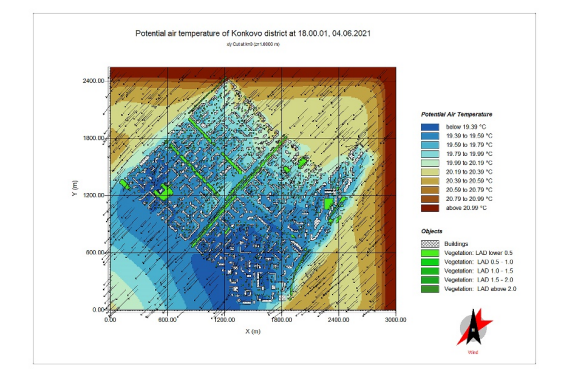


**Fig. 15.** Potential air temperature of Konkovo district at 04.00 am, June 04, 2021 yr.

**Fig. 16.** Potential air temperature of Konkovo district at 06.00 pm, June 04, 2021 yr.

The ENVI-met model also provides Mean Radiant Temperature (MRT) simulation results. MRT is used to measure the surrounding environmental temperature of a study object. This study chose the time with the lowest air temperature at 4:00 AM to represent the spatial distribution map of MRT in the Zamoskvorechye and Konkovo districts (Fig. 17, 18). After a day of exposure to natural factors such as sunlight, wind, and humidity, combined with anthropogenic factors like vehicular emissions and human activities, buildings and road surfaces absorb the most heat. At the time of the lowest air temperature, areas with heat accumulation reveal the locations of Urban Heat Islands (UHIs). These are high-density areas, enclosed high-rise buildings, poor natural ventilation in residential areas, limited or no green spaces, water bodies, and road surfaces with high Sky View Factors (SVFs).

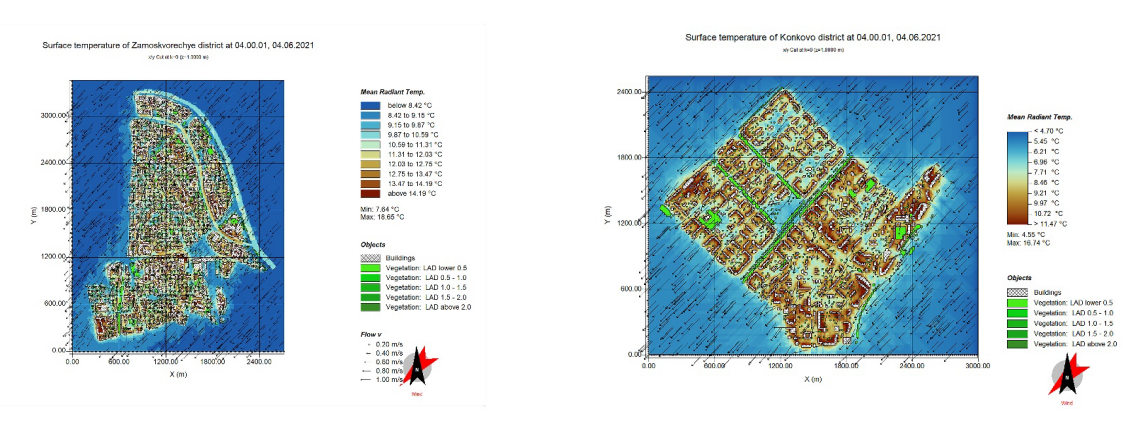


**Fig. 17.** The surface temperature of **Fig. 18.** The surface temperature of Konkovo Zamoskvorechye district at 04:00 am, June 04, district at 04:00 am, June 04, 2021 yr. 2021 yr.

# 3.3. Urban morphology and heat island intensity

The ENVI-met climate simulation model is a complex model that considers numerous urban parameters in combination with meteorological data, resulting in a high accuracy of R²=0.97. Therefore, this study proposes using simulation data to recalibrate the coefficients of the maximum urban heat island intensity equation proposed by Oke. Zamoskvorechye district is considered the urban centre, while the Konkovo district is considered a suburban area. The meteorological station in Konkovo district is taken as a reference, providing the temperature of the suburban area with a value of 19.91 °C at 4:00 PM. In the Zamoskvorechye district, 21 calculation points were selected on the road surface to recalibrate the coefficients of the Oke equation (Fig. 19, 20). Of the 21 chosen points, 11 were used for calibration, and 10 were used for validation. The time chosen to calculate the maximum urban heat island intensity of Zamoskvorechye district was 4:00 PM.

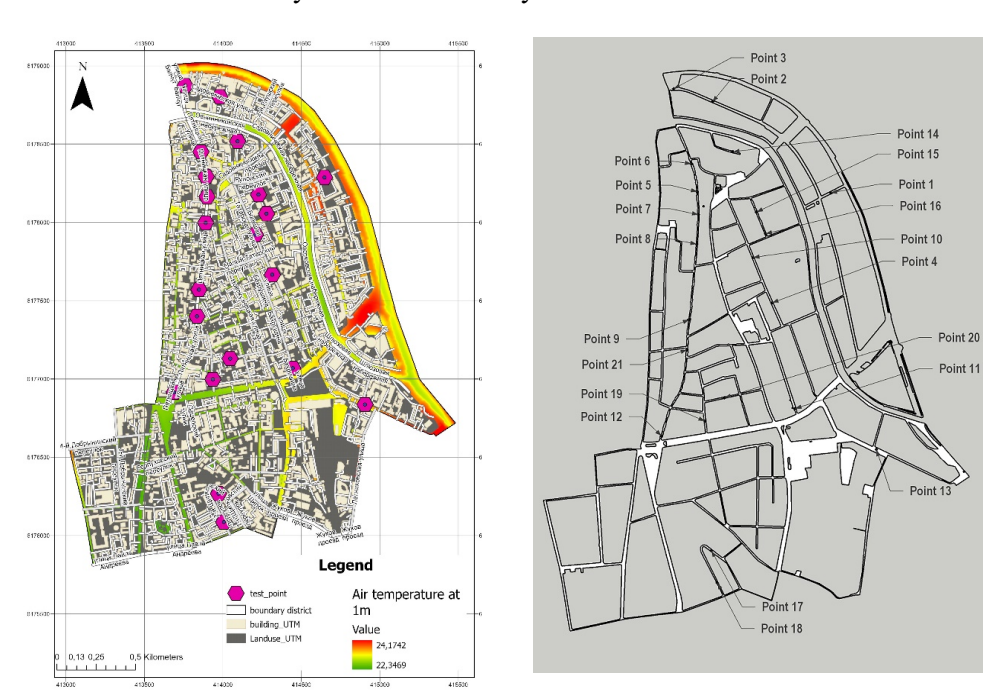


**Fig. 19.** Map of the surface temperature of roads in Zamoskvorechye district at 4 pm on June 4, 2021.

**Fig. 20.** Scheme of 21 calculated points on the road surface.

Table 8 presents urban indices and heat island intensity derived from integrating data from 3D GIS models and temperature indices obtained from climate simulation models of Zamoskvorechye and Konkovo districts.

The H/W ratios and urban heat island intensities of points 1 to 11 were used to calculate the coefficients of the Oke equation using nonlinear regression. The nonlinear regression equation is f(x) = a + b\*LN(x). Fig. 21 illustrates the nonlinear regression results between the H/W ratio and urban heat island intensity. The nonlinear regression results yielded an  $R^2$  value of 0.99. The empirical equation determined is:

$$\Delta t_{(u-r)} = 3.59 + 0.73 * LN(\frac{H}{W})$$
 (17)

Table 7. Parameters.

		Value	Standard Error	t-Value	Prob> t	Dependency
$\Delta t_{(u-r)}$	A	3.59	0.18025	19.91682	9.41944E-9	0.74716
	В	0.73592	0.3111	2.3655	0.04222	0.74716

Table 8 demonstrates a systematic overestimation of surface UHI intensity for points 1 to 21 when using Oke's equation (15), with values exceeding simulated values by 0.33 to 4.5 °C. However, if using the calibrated equation (17), which is more suitable for the urban morphology, the difference in urban heat island intensity compared to the simulation is from 0.01 to 0.6 °C.

Table 8. Calculation of simulated urban parameter and temperature indices.

Checkpoint	H <sub>average</sub> /W <sub>average</sub>	Sky view factor (SVF)	Air temperature at 1 m, (°C)	$\Delta t_{(\mathbb{W}-r)}$ $(^{\circ}\mathbb{C})$ (simulation)	\( \Delta t_{\left\lambda \text{\text{\$\pi \chi \text{\$\pi \chi \chi \text{\$\pi \chi \chi \text{\$\pi \chi \chi \chi \text{\$\pi \chi \chi \chi \chi \chi \chi \text{\$\pi \chi \chi \chi \chi \chi \chi \chi \ch	\( \Delta t_{\left\( \mu - r\right\)}\)  (\text{with} \)  modified \( \text{formula's} \)  Oke)
Point 1	0.61	0.64	23.46	3.55	5.45	3.22
Point 2	0.72	0.57	23.44	3.53	6.15	3.35
Point 3	0.88	0.49	23.38	3.47	6.96	3.50
Point 4	1.01	0.44	22.91	3.00	7.50	3.60
Point 5	0.40	0.78	23.02	3.11	3.86	2.93
Point 6	0.53	0.69	23.04	3.13	4.93	3.13
Point 7	0.56	0.66	22.92	3.01	5.17	3.17
Point 8	0.42	0.76	22.87	2.96	4.02	2.96
Point 9	0.34	0.83	22.72	2.81	3.14	2.80
Point 10	0.36	0,81	22.83	2.92	3.42	2.85
Point 11	0.40	0.78	22.97	3.06	3.85	2.93
Point 12	0.46	0.73	22.64	2.73	4.40	3.03
Point 13	0.42	0.77	23.18	3.27	3.96	2.95
Point 14	0.84	0.51	23.11	3.20	6.77	3.47
Point 15	0.87	0.50	22.93	3.02	6.89	3.49
Point 16	0.56	0.66	22.91	3.00	5.18	3.17
Point 17	0.61	0.64	22.65	2.74	5.47	3.23
Point 18	0.66	0.60	22.65	2.74	5.82	3.29
Point 19	0.70	0.58	22.68	2.77	6.04	3.33
Point 20	0.63	0.62	22.75	2.84	5.59	3.25
Point 21	0.62	0.63	22.81	2.90	5.53	3.24

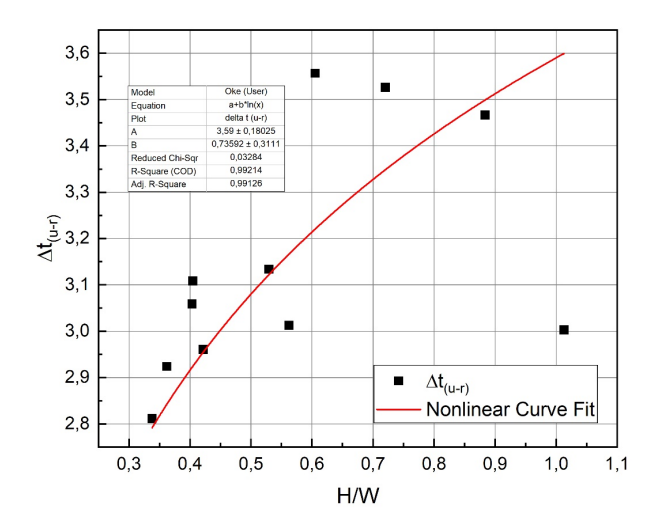


Fig. 21. Nonlinear regression graph between heat island intensity and H/W ratio.

#### Discussion

Cities are complex systems with many interacting factors influencing urban climate change. Therefore, measuring and differentiating their impacts remains challenging. Some previous studies have shown a reduction in radiation levels (W/m²) in canyons when the H/W ratio increases by increasing building height [57]. On the other hand, increasing the distance between buildings leads to a slight increase in radiation levels within canyons.

Our study applied the ENVI-met microclimate simulation model to recreate heat maps for the selected study areas, considering urban parameters combined with microclimate data from meteorological stations. This provided a consistent dataset of factors influencing the formation of urban heat islands. Additionally, the reconstructed surface temperature dataset helped optimise the coefficients in the Oke model to better suit the morphology of the selected study areas and increase accuracy. The simulation results for Zamoskvorechye and Konkovo districts showed that Zamoskvorechye, with an average height of 3 to 9 floors and a high building density, had a higher average temperature than Konkovo, which includes high-rise buildings (over ten floors) with an open structure.

#### Furture Studies

In this study, we successfully synchronized GIS database, microclimate data and 3D model of two districts of Moscow, and completed the construction of input data for ENVI-met microclimate numerical simulation model with high accuracy of information. The construction of 3D digital model with information synchronization with GIS database provides professional and non-professional users with the ability to perform simulation assessment of the interaction between microclimate and urban morphology easily and intuitively.

This study develops a digital simulation map based on real information through the city's geodatabase. The attribute data of buildings of the selected study area in CSV format of Arcgis software and its data entity model are combined and create a 3D model on Sketchup software.

Furthermore, the 3D digital model integrated with geographic information helps to make the simulation results of the impact assessment of urban morphology and urban heat island highly reliable. We believe that the method of building a 3D model to simulate microclimate and the relationship between heat island intensity and urban morphology presented in the article allows to shorten the time as well as improve the effectiveness of visualization and interaction between the urban environment and climate change. In addition, the model also allows to evaluate planning options under the impact of climate change, from which planners or policy makers can make appropriate adjustments to bring a more comfortable life to residents.

# 4. CONCLUSIONS

As one of Europe's largest and oldest cities, Moscow faces similar urban development and environmental challenges as other European metropolises. Its location in continental Europe makes it an ideal case study for investigating the impact of urban morphology on urban heat island (UHI) formation. This paper presents a methodology to assess the influence of urban indices on maximum UHI intensity and develops a numerical model tailored to the specific urban parameters of Moscow.

Using a climate simulation model to reconstruct temperature data, we can flexibly and cost-effectively investigate the relationship between the building height-to-width ratio (H/W) and maximum UHI intensity. Nonlinear regression analysis was employed to obtain a more accurate approximation and optimize the coefficients of the Oke model. Assessing maximum UHI intensity with sky view factor (SVF) and H/W ratio reveals that a high SVF allows for better air circulation, contributing to cooling and improved air quality. Additionally, high-rise buildings in urban areas can create a "rain-pumping" effect, increasing precipitation in surrounding areas. Moreover, a high SVF provides a sense of spaciousness and coolness, enhancing human comfort.

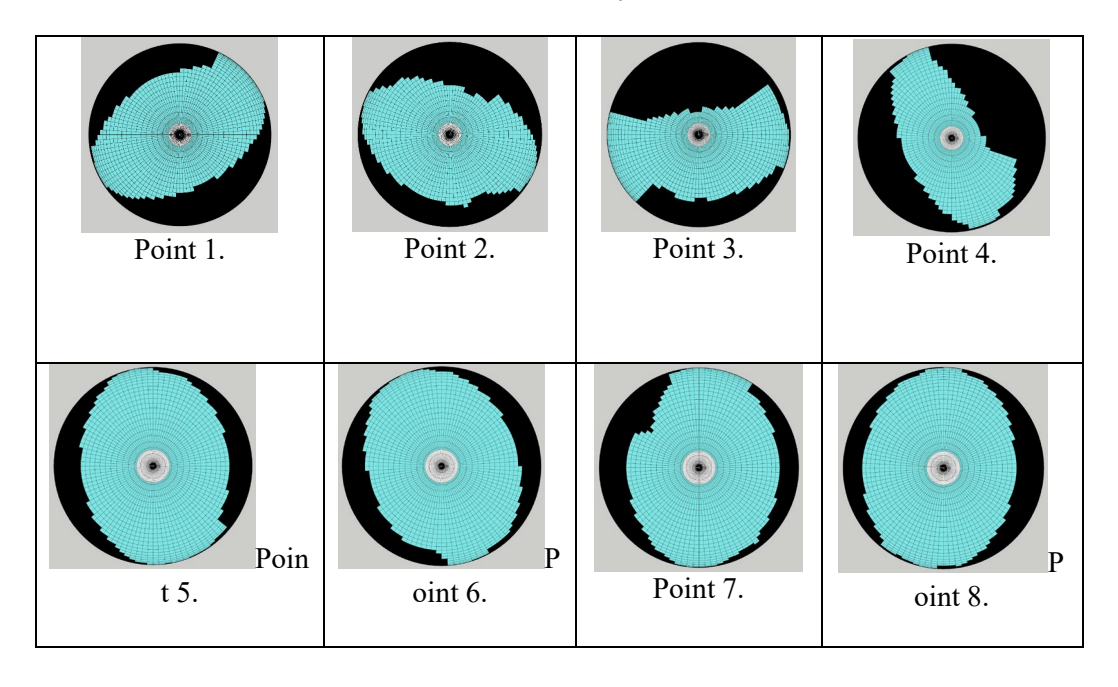
The findings highlight the importance of further research into the role of urban geometry in mitigating UHI effects. However, it is challenging to develop a universal equation for maximum UHI intensity applicable to all cities due to the complexity of urban morphology. Therefore, this paper presents a data collection and calculation methodology specific to a particular area. The proposed methodology can be adapted for studies in other locations.

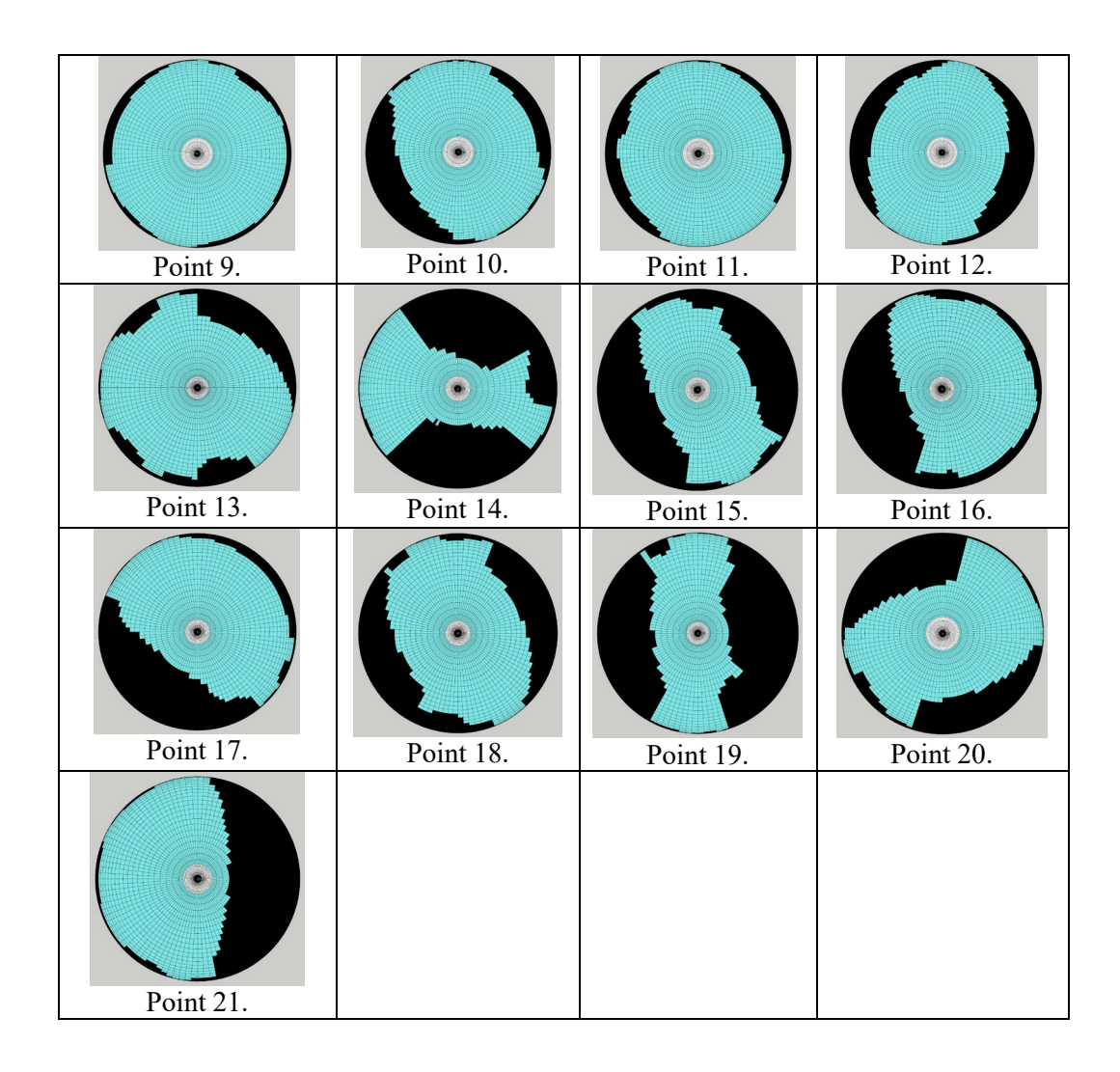
The practical significance of this research lies in providing a more accurate estimation of maximum UHI intensity tailored to the specific urban morphology, enabling the development of building design strategies that offer better thermal comfort for peoples.

#### 5. ACKNOWLEDGEMENTS

The research was funded by the National Research Moscow State University of Civil Engineering (grant for fundamental and applied scientific research, project No. 07-392/130)

Appendix A A1. Visualization of sky view factor





# REFERENCES

- [1] Stewart I.D., Oke T.R. Local climate zones for urban temperature studies. Bull Am Meteorol Soc. Dec. 2012. 93 (12) P. 1879 1900. doi: 10.1175/BAMS-D-11-00019.1
- [2] Chapman S., Watson J.E.M., Salazar A., Thatcher M., McAlpine C.A. The impact of urbanization and climate change on urban temperatures: a systematic review. Oct. 01, 2017. Springer Netherlands. doi: 10.1007/s10980-017-0561-4
- [3] Oke T.R. The energetic basis of the urban heat island, 1982.
- [4] Zhao L., Lee X., Smith R.B., Oleson K. Strong contributions of local background climate to urban heat islands. Nature. 2014. 511 (7508) P. 216 219. doi: 10.1038/nature13462
- [5] Grimm N.B. et al. Global Change and the Ecology of Cities. [Online]. Available: http://science.sciencemag.org/
- [6] Patz J.A., Campbell-Lendrum D., Holloway T., Foley J.A. Impact of regional climate change on human health. Nov. 17, 2005, Nature Publishing Group. doi: 10.1038/nature04188
- [7] Eliasson I.É. The use of climate knowledge in urban planning.
- [8] Tan J. et al. The urban heat island and its impact on heat waves and human health in Shanghai. Int J Biometeorol. Jan. 2010. 54 (1). P 75 84. doi: 10.1007/s00484-009-0256-x
- [9] Cao Q., Yu D., Georgescu M., Wu J., Wang W. Impacts of future urban expansion on summer climate and heat-related human health in eastern China. Environ Int. Mar. 2018. 12. P. 134 146. doi: 10.1016/j.envint.2017.12.027

- [10] Schatz J., Kucharik C.J. Urban climate effects on extreme temperatures in Madison, Wisconsin, USA. Environmental Research Letters. Sep. 2015. 10 (9). doi: 10.1088/1748-9326/10/9/094024
- [11] Li D., Bou-Zeid E. Synergistic Interactions between Urban Heat Islands and Heat Waves: The Impact in Cities Is Larger than the Sum of Its Parts\*". doi: 10.1175/JAMC-D-13-02.s1
- [12] Gabriel K.M.A., Endlicher W.R. Urban and rural mortality rates during heat waves in Berlin and Brandenburg, Germany. Environmental Pollution. Aug. 2011. 159 (8-9). P. 2044 2050. doi: 10.1016/j.envpol.2011.01.016
- [13] Marciotto E.R., Oliveira A.P., Hanna S.R. Modeling study of the aspect ratio influence on urban canopy energy fluxes with a modified wall-canyon energy budget scheme. Build Environ. Nov. 2010. 45 (11). P. 2497 2505. doi: 10.1016/j.buildenv.2010.05.012
- [14] L.W.A. van Hove, Jacobs C.M.J., Heusinkveld B.G., Elbers J.A., Van Driel B.L., Holtslag A.A.M. Temporal and spatial variability of urban heat island and thermal comfort within the Rotterdam agglomeration. Build Environ. Jan. 2015. 83. P. 91 103. doi: 10.1016/j.buildenv.2014.08.029
- [15] Li H., Zhou Y., Wang X., Zhou X., Zhang H., Sodoudi S. Quantifying urban heat island intensity and its physical mechanism using WRF/UCM. Science of the Total Environment. Feb. 2019. 650. P. 3110 3119. doi: 10.1016/j.scitotenv.2018.10.025
- [16] Zhou X., Chen H. Impact of urbanization-related land use land cover changes and urban morphology changes on the urban heat island phenomenon. Science of the Total Environment. Sep. 2018635. P. 1467 1476.. doi: 10.1016/j.scitotenv.2018.04.091
- [17] Dirksen M., Ronda R.J., Theeuwes N.E., Pagani G.A. Sky view factor calculations and its application in urban heat island studies. Urban Clim. Dec. 2019. 30. doi: 10.1016/j.uclim.2019.100498
- [18] Nasar-u-Minallah M., Haase D., Qureshi S., Zia S., Fatima M. Ecological monitoring of urban thermal field variance index and determining the surface urban heat island effects in Lahore, Pakistan. Environ Monit Assess. Oct. 2023. 195 (10). doi: 10.1007/s10661-023-11799-1
- [19] Qi Y., Li H., Pang Z., Gao W., Liu C. A Case Study of the Relationship Between Vegetation Coverage and Urban Heat Island in a Coastal City by Applying Digital Twins. Front Plant Sci. Apr. 2022. 13. doi: 10.3389/fpls.2022.861768
- [20] Zhou B., Rybski D., Kropp J.P. The role of city size and urban form in the surface urban heat island. Sci Rep. Dec. 2017. 7 (1). doi: 10.1038/s41598-017-04242-2
- [21] Duckworth F.S., Sandberg J.S. The Effect of Cities upon Horizontal and Vertical Temperature Gradients.
- [22] Makropoulou M. Microclimate improvement of Inner-city urban areas in a Mediterranean coastal city. Sustainability (Switzerland). May 2017. 9 (6). doi: 10.3390/su9060882
- [23] Akbari H. et al. Local climate change and urban heat island mitigation techniques The state of the art," Journal of Civil Engineering and Management Jan. 2016.. 22 (1). P. 1 16. doi: 10.3846/13923730.2015.1111934
- [24] Gago E.J., Roldan J., Pacheco-Torres R., Ordóñez J. The city and urban heat islands: A review of strategies to mitigate adverse effects. 2013. doi: 10.1016/j.rser.2013.05.057
- [25] Blocken B. Computational Fluid Dynamics for urban physics: Importance, scales, possibilities, limitations and ten tips and tricks towards accurate and reliable simulations. Build Environ. Sep. 2015. 91. P. 219 245. doi: 10.1016/j.buildenv.2015.02.015
- [26] Mirzaei P.A., Haghighat F. Approaches to study Urban Heat Island Abilities and limitations. Build Environ. Oct. 2010. 45 (10). P. 2192 2201. doi: 10.1016/j.buildenv.2010.04.001
- [27] Mirzaei P.A. Recent challenges in modeling of urban heat island. Dec. 01, 2015, Elsevier Ltd. doi: 10.1016/j.scs.2015.04.001
- [28] Pigeon G., Moscicki M.A., Voogt J.A., Masson V. Simulation of fall and winter surface energy balance over a dense urban area using the TEB scheme. Meteorology and Atmospheric Physics. 2008. 102 (3-4). P. 159 171. doi: 10.1007/s00703-008-0320-9

- [29] Thorsson S., Lindberg F., Eliasson I., Holmer B. Different methods for estimating the mean radiant temperature in an outdoor urban setting. in International Journal of Climatology, Nov. 2007. P. 1983 1993. doi: 10.1002/joc.1537
- [30] Mirzaei P.A., Haghighat F. Approaches to study Urban Heat Island Abilities and limitations," Build Environ. Oct. 2010. 45 (10). P. 2192 2201. doi: 10.1016/j.buildenv.2010.04.001
- [31] Botham-Myint D., Recktenwald G.W., Sailor D.J. Thermal footprint effect of rooftop urban cooling strategies. Urban Clim. Dec. 2015.14. P. 268 277. doi: 10.1016/j.uclim.2015.07.005
- [32] Lindberg F., Grimmond C.S.B. Nature of vegetation and building morphology characteristics across a city: Influence on shadow patterns and mean radiant temperatures in London. Urban Ecosyst. Nov. 2011. 14 (4). P. 617 634. doi: 10.1007/s11252-011-0184-5
- [33] Chow W.T.L., Brazel A.J. Assessing xeriscaping as a sustainable heat island mitigation approach for a desert city. Build Environ. Jan. 2012. 47 (1). P. 170 181. doi: 10.1016/j.buildenv.2011.07.027
- [34] Roth M., Lim V.H. Evaluation of canopy-layer air and mean radiant temperature simulations by a microclimate model over a tropical residential neighbourhood. Build Environ. Feb. 2017. 112. P. 177 189. doi: 10.1016/j.buildenv.2016.11.026
- [35] Singh M., Laefer D.F. Recent Trends and Remaining Limitations in Urban Microclimate Models. Open Urban Studies and Demography Journal. Feb. 2015. 1 (1) P. 1 12. doi: 10.2174/2352631901401010001
- [36] Michael Bruse and Heribert Fleer Simulating\_surface\_plant\_air\_interaction. Environmental Modelling & Software. 1998. 13 (3) P. 373 384.
- [37] Emmanuel R., Fernando H.J.S. Urban heat islands in humid and arid climates: Role of urban form and thermal properties in Colombo, Sri Lanka and Phoenix, USA. Clim Res. Sep. 2007. 34 (3) P. 241 251. doi: 10.3354/cr00694
- [38] Yang X., Zhao L., Bruse M., Meng Q. Evaluation of a microclimate model for predicting the thermal behavior of different ground surfaces. Build Environ. Feb. 2013. 60. P. 93 104. doi: 10.1016/j.buildenv.2012.11.008
- [39] Wang Y., Bakker F., R. de Groot, Wörtche H. Effect of ecosystem services provided by urban green infrastructure on indoor environment: A literature review. 2014, Elsevier Ltd. doi: 10.1016/j.buildenv.2014.03.021
- [40] Müller N., Kuttler W., Barlag A.B. Counteracting urban climate change: Adaptation measures and their effect on thermal comfort. Theor Appl Climatol. 2014. 115 (1-2). P. 243 257. doi: 10.1007/s00704-013-0890-4
- [41] Dimoudi A., Nikolopoulou M."Vegetation in the urban environment: microclimatic analysis and bene®ts.
- [42] Gatto E. et al. Impact of Urban vegetation on outdoor thermal comfort: Comparison between a Mediterranean city (Lecce, Italy) and a northern European city (Lahti, Finland). Forests Feb. 2020.. 11 (2). doi: 10.3390/f11020228
- [43] Erlwein S., Pauleit S. Trade-offs between urban green space and densification: Balancing outdoor thermal comfort, mobility, and housing demand. Urban Plan. 2021. 6 (1). P. 5 19. doi: 10.17645/UP.V6I1.3481
- [44] Coutts A.M., Beringer J., Tapper N.J. Impact of increasing urban density on local climate: Spatial and temporal variations in the surface energy balance in Melbourne, Australia. J Appl Meteorol Climatol. Apr. 2007. 46 (4). P. 477 493. doi: 10.1175/JAM2462.1
- [45] Elansky N.F., Lavrova O.V., Rakin A.A., Skorokhod A.I. Anthropogenic disturbances of the atmosphere in Moscow region. Doklady Earth Sciences. 2014. 454 (2). P. 158 162. doi: 10.1134/S1028334X14020020
- [46] Lee H., Mayer H., Chen L. Contribution of trees and grasslands to the mitigation of human heat stress in a residential district of Freiburg, Southwest Germany. Landsc Urban Plan Apr. 2016.. 148. P. 37 50. doi: 10.1016/j.landurbplan.2015.12.00

- [47] Sharmin T., Steemers K., Matzarakis A. Microclimatic modelling in assessing the impact of urban geometry on urban thermal environment. Sustain Cities So. Oct. 2017. 34. P. 293 308. doi: 10.1016/j.scs.2017.07.006
- [48] Toparlar Y., Blocken B., Maiheu B., van Heijst G.J.F. A review on the CFD analysis of urban microclimate. 2017. Elsevier Ltd. doi: 10.1016/j.rser.2017.05.248
- [49] Acero J.A., Herranz-Pascual K. A comparison of thermal comfort conditions in four urban spaces by means of measurements and modelling techniques. Build Environ. Nov. 2015. 93 (P2). P. 245 257. doi: 10.1016/j.buildenv.2015.06.028
- [50] Morakinyo T.E., Kong, L. Lau K.K.L., Yuan C., Ng E. A study on the impact of shadow-cast and tree species on in-canyon and neighborhood's thermal comfort. Build Environ. Apr. 2017. 115. P. 1 17. doi: 10.1016/j.buildenv.2017.01.005
- [51] Liu J., Chen J.M., Black T.A., Novak M.D. E-E modelling of turbulent air flow downwind of a model forest edge \*\* Corresponding author, and presently with Canada Centre for Remote Sensing," 1996.
- [52] Tetsuji Yamada A numerical model study of turbulent airflow in and above a forest canopy. Journal of the Meteorological Society of Japan. 1982.60 (1). P. 439 454. doi: 10.2151/jmsj1965.60.1 439
- [53] Tetsuji Yamada and George Mellor A simulation of the Wangara atmospheric boundary layer data. J Atmos Sci. 1975. 32. P. 2309 2329. doi: 10.1175/1520-0469(1975)032<2309:ASOTWA>2.0.CO;2
- [54] Zheng Y.et al. GIS-based mapping of Local Climate Zone in the high-density city of Hong Kong. Urban Clim. Jun. 2018. 24. P. 419 448. doi: 10.1016/j.uclim.2017.05.008.
- [55] Unal Cilek M., Cilek A. Analyses of land surface temperature (LST) variability among local climate zones (LCZs) comparing Landsat-8 and ENVI-met model data. Sustain Cities Soc. Jun. 2021. 69. doi: 10.1016/j.scs.2021.102877
- [56] Chen L.et al. Sky view factor analysis of street canyons and its implications for daytime intra-urban air temperature differentials in high-rise, high-density urban areas of Hong Kong: A GIS-based simulation approach. International Journal of Climatology. 32 (1). 2012. P. 121 136. doi: 10.1002/joc.2243
- [57] Theeuwes N.E., Steeneveld G.J., Ronda R.J., Heusinkveld B.G., L.W.A. van Hove, Holtslag A.A.M. Seasonal dependence of the urban heat island on the street canyon aspect ratio. Quarterly Journal of the Royal Meteorological Society. Oct. 2014. 140 (684). P. 2197 2210. doi: 10.1002/qj.2289

#### INFORMATION ABOUT THE AUTHORS

Le M.T., e-mail: architect290587@gmail.com, ORCID ID: https://orcid.org/0000-0003-4164-7452, SCOPUS: https://www.scopus.com/authid/detail.uri?authorId=57208299011, National Research Moscow State University of Civil Engineering, Ph.D of the Urban planning Department

**Bakaeva N.V.,** e-mail: natbak@mail.ru, ORCID ID: https://orcid.org/0000-0003-0518-6521, SCOPUS: https://www.scopus.com/authid/detail.uri?authorId=56826095700, National Research Moscow State University of Civil Engineering, Doctor of Engineering Sciences, Professor of the Urban planning Department